ResearchGate

See discussions, stats, and author profiles for this publication at: https://www.researchgate.net/publication/45404806

Periodic Si Nanopillar Arrays Fabricated by Colloidal Lithography and Catalytic Etching for Broadband and Omnidirectional Elimination of Fresnel Reflection

ARTICLE *in* LANGMUIR · AUGUST 2010

Impact Factor: 4.46 · DOI: 10.1021/la1012507 · Source: PubMed

CITATIONS
55

READS
39

5 AUTHORS, INCLUDING:

Hsin-Ping Wang

19 PUBLICATIONS **273** CITATIONS

SEE PROFILE

K. Y. Lai

National Central University

45 PUBLICATIONS **555** CITATIONS

SEE PROFILE

Available from: K. Y. Lai
Retrieved on: 31 January 2016

Langmuir Article

pubs.acs.org/Langmuir
© 2010 American Chemical Society

Periodic Si Nanopillar Arrays Fabricated by Colloidal Lithography and Catalytic Etching for Broadband and Omnidirectional Elimination of Fresnel Reflection

Hsin-Ping Wang,[†] Kun-Yu Lai,[†] Yi-Ruei Lin,[†] Chin-An Lin,[†] and Jr-Hau He*[,†,§]

[†]*Institute of Photonics and Optoelectronics and* [§]*Department of Electrical Engineering, National Taiwan University, Taipei, 106 Taiwan, ROC*

Received March 30, 2010. Revised Manuscript Received June 18, 2010

Periodic Si nanopillar arrays (NPAs) were fabricated by the colloidal lithography combined with catalytic etching. By varying the size of colloidal crystals using oxygen plasma etching, Si NPAs with desirable diameter and fill factor could be obtained. The Fresnel reflection can be eliminated effectively over broadband regions by NPAs; i.e., the wavelength-averaged specular reflectance is decreased to 0.70% at wavelengths of 200−1900 nm. The reflectance is reduced greatly for the incident angles up to 70° for both s- and p-polarized light. These excellent antireflection performances are attributed to light trapping effect and very low effective refractive indices, which can be modified by the fill factor of Si in the NPA layers.

Introduction

Much effort has been devoted not only to synthesize Si nanowires (NWs) with a controlled density and the regularity in terms of diameters and lengths, but also to accurately position NWs in arrays for a variety of practical applications of nanomaterials,[1] such as field-effect transistors,[2] field emitters,[3,4] solar cells,[5] and biosensors.[6]

The most common method for the synthesis of Si NWs is the vapor−liquid−solid (VLS) method. However, several challenges for practical applications of VLS-synthesized Si NWs remain. For example, the severe diffusion of catalyst metal, typically Au, into Si during the NW growth is inevitable and detrimental to the realization of Si NW devices due to Au contamination in Si, creating carrier traps and reducing minority carrier lifetimes. Another concern is the orientation control since the orientation of VLS-synthesized Si NWs depends on the wire dimension greatly,[7,8] which limits the integration of Si NWs with current complementary metal−oxide−semiconductor (CMOS) technology. On the other hand, metal-assisted wet etching via the electrochemical reaction can produce Si NWs oriented along the ⟨100⟩ direction with the advantage of being a scalable, room temperature process without metal contamination.[9−11] Recently, metal-assisted wet etching in combination with various metal patterning techniques, such as nanoscale copolymer lithography[12,13] and anodic aluminum oxide,[14] has been demonstrated as a promising method to control the position, size, and geometry of NWs.

For Si-based optoelectronic devices, such as displays, photodetectors, and solar cells, the high reflective index of Si results in up to 40% of the incident light reflected, which severely limits device performance.[15] Suppressing the undesired Fresnel reflection generated at the interfaces is crucial. As compared to single- or multilayered dielectrics with various problems, such as poor adhesion, limited working wavelength range, and thermal instability,[16] Si NWs with a periodicity similar to the wavelength of incident light have been demonstrated as an alternative to eliminate the Fresnel reflection over a broad wavelength and field of view.[17,18] The surface textures of the NW layers can effectively enhance light trapping,[19] and further reduce the surface reflectance since the NW layers behave like an effective homogeneous medium with an intermediate refractive index, n_{eff}, between air and Si, which avoids the abrupt index transition at the air/Si interface.[20] Furthermore, Xi et al. reported that silica NW arrays on Si substrates with a refractive index of 1.08 are smaller than those of the lowest refractive-index materials available in nature, such as magnesium fluoride (n = 1.39) and silica (n = 1.46).[21] The materials with low refractive indices are highly desirable for many photonic devices involving antireflection or high-reflection coating, resonant cavity, photonic crystal structures, and solar cells.[21,22]

*To whom correspondence should be addressed. E-mail: jhhe@cc.ee.ntu.edu.tw.

(1) Zhang, X. Y.; Zhang, L. D.; Meng, G. W.; Li, G. H.; Jin-Phillipp, N. Y.; Phillipp, F. *Adv. Mater.* **2001**, *13*, 1238–1241.
(2) Goldberger, J.; Hochbaum, A. I.; Fan, R.; Yang, P. D. *Nano Lett.* **2006**, *6*, 973–977.
(3) Fang, X. S.; Bando, Y.; Gautam, U. K.; Ye, C.; Golberg, D. *J. Mater. Chem.* **2008**, *18*, 509–522.
(4) Fang, X. S.; Bando, Y.; Ye, C. H.; Shen, G. Z.; Gautam, U. K.; Tang, C. C.; Golberg, D. *Chem. Commun.* **2007**, 4093–4095.
(5) Zhu, J.; Hsu, C.-M.; Yu, Z.; Fan, S.; Cui, Y. *Nano Lett.* **2009**, *10*, 1979–1984.
(6) Wanekaya, A. K.; Chen, W.; Myung, N. V.; Mulchandani, A. *Electroanalysis* **2006**, *18*, 533–550.
(7) Schmidt, V.; Senz, S.; Gosele, U. *Nano Lett.* **2005**, *5*, 931–935.
(8) Cui, Y.; Lauhon, L. J.; Gudiksen, M. S.; Wang, J. F.; Lieber, C. M. *Appl. Phys. Lett.* **2001**, *78*, 2214–2216.
(9) Smith, R. L.; Collins, S. D. *J. Appl. Phys.* **1992**, *71*, R1–R22.
(10) Peng, K. Q.; Huang, Z. P.; Zhu, J. *Adv. Mater.* **2004**, *16*, 73–76.
(11) Chen, C. Y.; Wu, C. S.; Chou, C. J.; Yen, T. J. *Adv. Mater.* **2008**, *20*, 3811–3815.
(12) Chang, S. W.; Chuang, V. P.; Boles, S. T.; Ross, C. A.; Thompson, C. V. *Adv. Funct. Mater.* **2009**, *19*, 2495–2500.
(13) Huang, Z. P.; Fang, H.; Zhu, J. *Adv. Mater.* **2007**, *19*, 744–748.
(14) Huang, Z. P.; Zhang, X. X.; Reiche, M.; Liu, L. F.; Lee, W.; Shimizu, T.; Senz, S.; Gosele, U. *Nano Lett.* **2008**, *8*, 3046–3051.
(15) Doshi, P.; Jellison, G. E.; Rohatgi, A. *Appl. Opt.* **1997**, *36*, 7826–7837.
(16) Hadobas, K.; Kirsch, S.; Carl, A.; Acet, M.; Wassermann, E. F. *Nanotechnology* **2000**, *11*, 161–164.
(17) Huang, J. Y.; Wang, X. D.; Wang, Z. L. *Nano Lett.* **2006**, *6*, 2325–2331.
(18) Xi, J. Q.; Schubert, M. F.; Kim, J. K.; Schubert, E. F.; Chen, M. F.; Lin, S. Y.; Liu, W.; Smart, J. A. *Nat. Photonics* **2007**, *1*, 176–179.
(19) Sai, H.; Kanamori, Y.; Arafune, K.; Ohshita, Y.; Yamaguchi, M. *Prog. Photovoltaics* **2007**, *15*, 415–423.
(20) Clapham, P. B.; Hutley, M. C. *Nature* **1973**, *244*, 281–282.
(21) Xi, J. Q.; Kim, J. K.; Schubert, E. F. *Nano Lett.* **2005**, *5*, 1385–1387.
(22) Lin, S. Y.; Chow, E.; Hietala, V.; Villeneuve, P. R.; Joannopoulos, J. D. *Science* **1998**, *282*, 274–276.

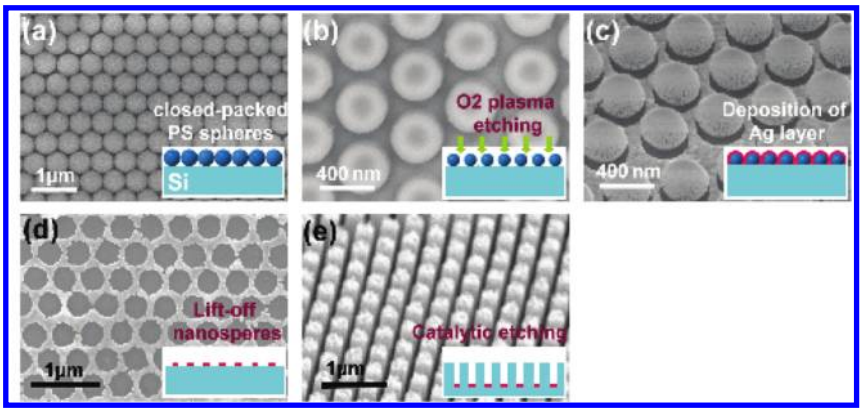

Figure 1. SEM images at various stages for fabricating periodic Si NPAs. The insets are the schematics of the corresponding experimental procedures.

In this study, periodic Si nanopillar arrays (NPAs) are synthesized using catalytic wet etching integrating with colloidal lithography. In this process, a hexagonal array of nanospheres, whose diameter can be modified by oxygen plasma etching, is employed as the patterning mask for Ag deposition on Si substrates. The NPA structures are achieved by the subsequent catalytic wet etching with Ag patterns. Si NPAs with well-controlled geometric features significantly eliminate the Fresnel reflection over wavelengths from 200 to 1900 nm and angles of incidence (AOIs) up to 70°. This is achieved by controlling the refractive index of the Si NPA layer down to a minimum value of $n_{\text{eff}} = 1.18$.

Results and Discussion

Figure 1 describes the fabrication procedures of Si NPAs. The antireflection characteristics of the Si NW structures under solar illumination would be optimum when the periodicity of Si NWs (NW-to-NW distance) is around 500 nm.[19,23] Therefore, the periodicity of Si NPAs is chosen to be 500 nm, predefined by the diameter of nanospheres. As shown in Figure 1a, the cleaned Si substrates were drop-coated with a monolayer of 500-nm polystyrene (PS) nanospheres, which has been described elsewhere.[24] The nanospheres were shrunk by oxygen plasma for the duration from 150 to 210 to 240 s, as shown in Figure 1b. Subsequently, a 40-nm-thick Ag layer was deposited on the nanosphere-coated substrates using electron beam evaporation (Figure 1c). After the deposition of Ag films, the films on top of the PS nanospheres were lifted off by removing the nanospheres in an ultrasonic bath, and thereby the honeycomb-like pattern of Ag layers was obtained (Figure 1d). The Si NPAs were finally achieved by immersing the patterned substrates in the etching solution of HF/H_2O_2 for 5 min (Figure 1e). The Si NPAs fabricated by well-defined colloidal lithography exhibit uniform features and periodicity. The formation of Si NPAs results from the galvanic displacement, which contains Ag-induced local oxidation and subsequent dissolution of Si. In analogy with the pioneering studies of Si etching,[25,26] the mechanism of the galvanic process can be summarized by two half-cell reactions:

Cathode reaction at the metal:

$$H_2O_2 + 2H^+ \rightarrow 2H_2O + 2h^+$$

$$2H^+ + 2e^- \rightarrow H_2$$

Anode reaction at the Si:

$$Si + 2H_2O + 4h^+ \rightarrow SiO_2 + 4H^+$$

$$SiO_2 + 6HF \rightarrow H_2SiF_6 + 2H_2O$$

Overall reaction:

$$Si + H_2O_2 + 6HF \rightarrow 2H_2O + H_2SiF_6 + H_2$$

In the process, the Ag layers adhering to Si surfaces have a greater electronegativity than Si, and thus electrons are attracted from Si to Ag, making the Ag layers negatively charged. Subsequently, the O^- ions (acting as free holes, h^+) from H_2O_2 capture electrons preferentially from the negatively charged Ag layers and become O^{2-} ions. This charge transfer causes the local oxidation of the Si underneath the Ag patterns. The produced SiO_2 is then continuously etched away by HF, leading to the penetration of Ag into Si substrates. As a result, the pattern defined by PS nanospheres is transferred to the substrates, and eventually the Si NPAs are obtained when the Ag penetration reaches a certain depth. Since h^+ derives from H_2O_2, these reactions indicate that Si NPAs of similar geometric features can be generated regardless of doping types and level of Si substrates.[26] This is in contrast to the wet etching using Ag^+ redox in $AgNO_3$ solutions, where the Ag^+ ions approaching Si surfaces tend to be attracted by the randomly distributed Ag nuclei (negatively charged), and the rate of chemical etching varies with different sizes of Ag particles,[10] resulting in Si NWs of irregular distributions and lengths.[26]

Figure 2a−c shows the scanning electron microscopy (SEM) images (recorded at a tilted angle of 45°) of as-synthesized Si NPAs. The insets in Figure 2a−c are the corresponding nanospheres after the oxygen plasma etching for various durations. The diameters of the NPAs in Figure 2a−c are determined to be 385, 278, and 187 nm, respectively. Figure 2d is a typical cross-sectional SEM image of Figure 2b, showing the uniformity of etching profiles. The length of Si NPAs is estimated to be 2.2 μm for all samples. The slightly

(23) Li, J. S.; Yu, H. Y.; Wong, S. M.; Zhang, G.; Sun, X. W.; Lo, P. G. Q.; Kwong, D. L. *Appl. Phys. Lett.* **2009**, *95*, 033102–033102−3.
(24) Hsieh, H. Y.; Huang, S. H.; Liao, K. F.; Su, S. K.; Lai, C. H.; Chen, L. J. *Nanotechnology* **2007**, *18*, 505305.
(25) Li, X.; Bohn, P. W. *Appl. Phys. Lett.* **2000**, *77*, 2572–2574.
(26) Peng, K. Q.; Hu, J. J.; Yan, Y. J.; Wu, Y.; Fang, H.; Xu, Y.; Lee, S. T.; Zhu, J. *Adv. Funct. Mater.* **2006**, *16*, 387–394.

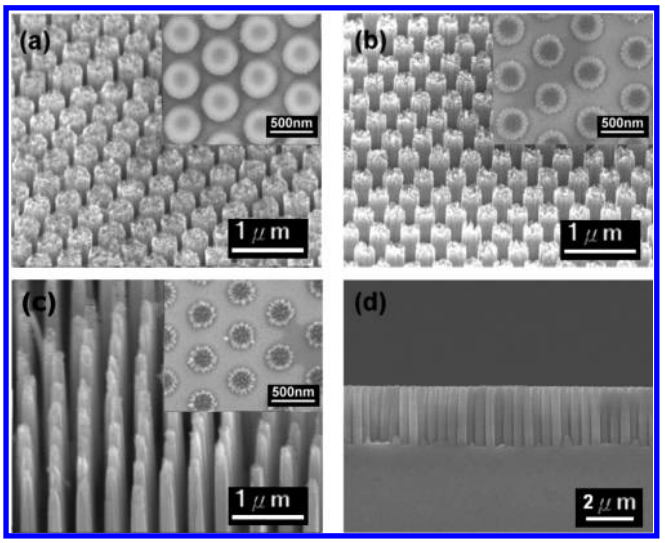

Figure 2. The 45°-tilted SEM images of Si NPAs produced by Ag-assisted wet etching for 5 min with PS nanospheres whose diameters are controlled by oxygen plasma etching for (a) 150 s, (b) 210 s, and (c) 240 s, and the insets are the SEM images of the corresponding nanospheres. (d) A typical cross-sectional SEM image of panel b.

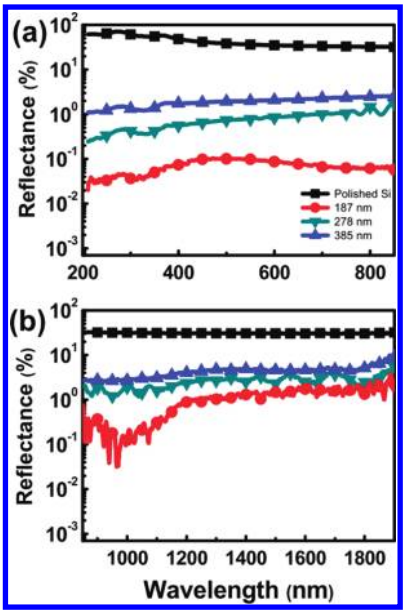

Figure 3. Specular reflectance of Si NPAs over wavelength regions of (a) 200−850 nm and (b) 850−1900 nm.

tapered morphology is especially pronounced in NPAs with small diameters. This might be due to the fact that as the Si substrates are exposed to the etching solution for a longer time, more Ag (Ag^+/Ag, redox potential of 0.80 V vs normal hydrogen electrode (NHE)) is oxidized and dissolved into the solution containing H_2O_2 (redox potential of 1.72 V vs NHE in a solution at pH = 0.3),[27,28] or the slight isotropic etching causes smaller diameters of the tip parts.[10] The coverage of NPAs is characterized by the fill factor (FF), which is defined by the area ratio of NPAs to the entire substrate surfaces using the top-view SEM images. The FFs of Figure 2a−c are 0.54, 0.28, and 0.13, respectively.

In order to evaluate the elimination of the Fresnel reflection, the specular reflectance of Si NPAs in the wavelength range of 200−1900 nm was measured, as shown in Figure 3. In contrast to the polished Si wafer exhibiting reflectance above 30% due to the high refractive index from UV to near-infrared regions, the periodic Si NPAs effectively reduce the reflectance over the broadband regions, and the reflectance decreases with decreasing the diameters of NPAs. For the 187-nm NPAs, the reflectance remains under 0.10% and 2.25% at 380−850 nm and 850−1800 nm, respectively. As the wavelength of incident light is much higher than the periodicity of the NPAs, effective medium theory can be used to explain the low reflectance achieved by the Si NPAs.[29] We note that several effective medium approximations (EMAs) were examined, and exhibit similar trends to what is discussed below. The n_{eff} of Si NPAs is calculated by the Bruggeman EMA:[29]

$$f_{Si}\frac{n_{Si}^2 - n_{eff}^2}{n_{Si}^2 + 2n_{eff}^2} + (1 - f_{Si})\frac{n_{air}^2 - n_{eff}^2}{n_{air}^2 + 2n_{eff}^2} = 0 \qquad (2)$$

where f_{si} is the FF of Si NPAs, and n_{Si} and n_{air} are the refractive indices of Si and air, respectively. With n_{Si} = 3.5 and n_{air} = 1, the calculated n_{eff}'s of the structures shown in Figure 2a−c are 2.27, 1.51, and 1.18, respectively. These intermediate n_{eff} values between those of Si and air result in the reduced reflectance by avoiding the abrupt transition from air to Si. Compared with the values of other samples, the smallest n_{eff} of the 187-nm Si NPAs is closest to the air, allowing the most incident light going through the air/Si NPAs interface. Moreover, the most tapered morphology of the 187-nm NPAs indicates the most grading in n_{eff}.[30] Both of these features give rise to the lowest reflectance achieved by the 187-nm NPAs. When the wavelength of incident light is smaller than or comparable to the periodicity of the NPAs, the light splits off to several diffraction orders, and the multiple scattering light paths are folded up inside the NPA structures, which increases the absorptance[31] and therefore suppresses the reflectance. According to the SEM images shown in Figure 2, the average air gap between nanopillars (~313 nm) in the 187-nm Si NPAs is the largest among the three samples, leading to the most light entering the NPA layers. In addition, the reduced tip area of the sharpened nanopillars would make the incident light less likely to be reflected on the flat top of NPAs. Therefore, the most significantly suppressed reflection is obtained with 187-nm Si NPAs at short wavelengths. The slightly increased reflectance beyond 1100 nm is attributed to the low absorption below the band gap of the silicon (1100 nm).[32]

It is worth noting that the diameter-dependence of reflectance shown here is consistent with the simulation results reported by Hu et al.,[33] but contrary to those published by Lin et al.[34] This discrepancy is believed to be caused by the large difference in nanopillar lengths, which are respectively 2.3 and 2.2 μm in Hu's and the present work, but only 0.2 μm in Lin's. For short (0.2 μm) Si NPAs, the incident light essentially sees a rough surface instead of a pillar forest. In this case, increasing the diameters of nanopillars makes the surface rough, and thus enhances light trapping by increasing the opportunity for the reflected light to bounce

(27) Li, Y. F.; Zhang, J. H.; Zhu, S. J.; Dong, H. P.; Wang, Z. H.; Sun, Z. Q.; Guo, J. R.; Yang, B. *J. Mater. Chem.* **2009**, *19*, 1806–1810.
(28) Lee, C. L.; Tsujino, K.; Kanda, Y.; Ikeda, S.; Matsumura, M. *J. Mater. Chem.* **2008**, *18*, 1015–1020.
(29) Mohring, H. D.; Abel, C. D.; Bruggemann, R.; Bauer, G. H. *J. Non-Cryst. Solids* **1991**, *137*, 847–850.
(30) Zhu, J.; Yu, Z. F.; Burkhard, G. F.; Hsu, C. M.; Connor, S. T.; Xu, Y. Q.; Wang, Q.; McGehee, M.; Fan, S. H.; Cui, Y. *Nano Lett.* **2009**, *9*, 279–282.
(31) Poruba, A.; Fejfar, A.; Remes, Z.; Springer, J.; Vanecek, M.; Kocka, J.; Meier, J.; Torres, P.; Shah, A. *J. Appl. Phys.* **2000**, *88*, 148–160.
(32) Chattopadhyray, S.; Chen, L. C.; Chen, K. H. *Crit. Rev. Solid State* **2006**, *31*, 15–53.
(33) Hu, L.; Chen, G. *Nano Lett.* **2007**, *7*, 3249–3252.
(34) Lin, Y. R.; Wang, H. P.; Lin, C. A.; He, J. H. *J. Appl. Phys.* **2009**, *106*, 114310–114310−4.

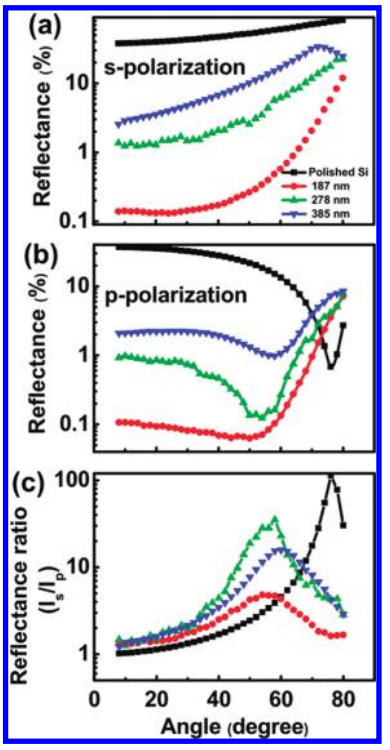

Figure 4. Specular reflectance as a function of AOI for (a) s-polarized and (b) p-polarized light with a wavelength of 528 nm. (c) The specular reflectance ratio of the s-polarized to p-polarized light (I_s/I_p) as a function of AOI with a wavelength of 528 nm.

between the nanopillars,[34] resulting in the low reflectance. On the other hand, for significantly lengthened Si NPAs in the present study, the suppression of reflectance is mainly determined by how much incident light enters the NPAs. Decreasing the nanopillar diameters facilitates the light traveling from air to NPAs as a result of the small n_{eff} and large air gaps, leading to a low reflectance.

Since sunlight strikes the Earth surface from different directions during the day, a desirable feature of any antireflection coating for solar cells is the Fresnel reflection suppression over the wide AOIs, which is called omnidirectionality. To evaluate the Si NPAs fabricated by colloidal lithography and wet etching, the specular reflectance at different AOIs with s- and p-polarized light was measured, as shown in Figure 4a,b. For the polished Si substrates, the reflectance varies strongly with AOI for s- and p-polarized light. In contrast, NPAs are effective to eliminate angular reflection and insensitive to the polarization of light. The reflectance is generally reduced with decreasing diameters of Si NPAs over a wide range of AOIs for both s- and p-polarized light. The reflectance of 187-nm Si NPAs measured with s-, and p-polarized light for AOI up to 70° remains below 2.06%, and 1.75%, respectively. These values are lower than those of a polished Si surface by more than one order, demonstrating the excellent omnidirectionality of Si NPAs. It is noticed that the reflectance of all NPA structures is noticeably increased after AOI reaches 60°. This trend can be attributed to the increased scattering of the incident light at large AOIs.[35] Intuitively, when the light reaches the Si NPA surfaces at a large AOI, the portion of the light entering the NPA layers is decreased, suggesting that the probability of trapping light within the NPA layers is reduced, and therefore the reflectance is increased. The polarization-dependent omnidirectionality can be characterized by the ratio of the reflectance of the s-polarization to that of the p-polarization (I_s/I_p), as presented in Figure 4c. The polished Si exhibits a maximum of $I_s/I_p = 113.3$, while a maximum of I_s/I_p is decreased to less than 4.8 for 187-nm Si NPA structures, suggesting that the reflection becomes polarization-insensitive on the Si NPAs over a wide range of AOIs. Brewster's angle (BA) can be easily identified by the AOI giving the highest I_s/I_p value. One can see that BA shifts from 76° on the polished surface to less than 58° at the nanostructured surfaces. The shift is due to the incoherent multiple scattering at a rough surface.[36]

Conclusion

We reported that periodic Si NPAs were formed by colloidal lithography combined with metal-assisted wet chemical etching. By varying the diameters of colloidal crystals using oxygen plasma etching, Si NPAs with controlled diameter and FF could be obtained. The Si NPA layer with an effective refractive index as low as 1.18 virtually eliminates the Fresnel reflection over a broad wavelength (200−1900 nm) and AOI (up to 70°). A maximum I_s/I_p as low as 4.8 for 187-nm Si NPA structures indicates the polarization-insensitive reflection on the Si NPAs over a wide range of AOIs.

Experimental Section

Nanosphere lithography was used to pattern Si NPAs. Si samples were cut from single crystalline p-type (001) Si substrates with $\rho = 8-12\ \Omega\cdot$cm. For preparing a hydrophilic surface, the samples were cleaned in acetone and then in a solution of H_2SO_4/H_2O_2 at 80 °C for 10 min. A solution with 500-nm PS nanospheres was then drop-coated on the Si samples and dried at 50 °C and 87.5% humidity. A close-packed hexagonal PS monolayer was formed upon drying of the solution. Oxygen plasma etching was applied to shrink the diameters using SAMCO RIE-10NR. A 40-nm-thick Ag layer was deposited on the patterned substrates using electron beam evaporation in the chamber pressure lower than 1×10^{-6} Torr. After lifting off PS nanospheres, metal-assisted wet etching was carried out by immersing the Ag-patterned Si substrates in a solution of HF/H_2O_2 for 5 min to obtain the NPA structures.

Morphological studies of the Si NPAs were performed with a JEOL JSM-6500 field emission SEM. Specular reflectance over the wavelength regions from 200 to 1900 nm was measured by a JASCO V-670 UV−vis−IR spectrometer with AOI fixed at 8°. The omnidirectional property of the antireflective Si NPAs was characterized by reflection at the AOI from 5° to 80° with a fixed incident wavelength of 528 nm. During the measurements, s- and p-polarized light was used, where s and p denote the incidence planes perpendicular and parallel to the electric field of the incident light, respectively.

Acknowledgment. The research was supported by the National Science Council Grant No. NSC 96-2112-M-002-038-MY3, NSC 96-2622-M-002-002-CC3, and Aim for Top University Project from the Ministry of Education.

(35) Kanamori, Y.; Sasaki, M.; Hane, K. *Opt. Lett.* **1999**, *24*, 1422–1424.

(36) Kawanishi, T. *Opt. Commun.* **2000**, *186*, 251–258.